MECSOL Joinville 2017
April 26-28, 2017
Joinville, Santa Catarina, Brazil

Sensitivity Analysis for Topology Optimization of Nonlinear Fluid Actuators

Daniel Candeloro Cunha
Department of Computational Mechanics
Faculty of Mechanical Engineering, Unicamp
cunha@fem.unicamp.br

Renato Pavanello
Department of Computational Mechanics
Faculty of Mechanical Engineering, Unicamp
pava@fem.unicamp.br

ABSTRACT

Some biological cellular systems behave as highly energy-efficient fluid actuators with very desirable features, as lightweight, simple input and large actuation. Seeking such features, this work developed the primary stages for designing bio-inspired fluid actuators, based on nastic plants.

For modeling the system, it was considered a continuum solid structure of homogeneous and isotropic material with linear stress-strain relationship, internally loaded by pressured fluid cavities. The compliant mechanism transmits, through a transmittance ratio, the available pressure energy to a set of specified springs, whose total strain energy represents the output work. In current approach, the fluid was stationary and the input pressure was the same for all cavities. Two nonlinear aspects were considered. Geometrical nonlinearity, since compliant mechanisms are expected to work under finite displacements. And load nonlinearity, since the loads depend on the deformed structure configuration.

The mechanism outlines were described and its finite element model was developed and validated. Furthermore, aiming for the design of those actuators through topology optimization techniques, a sensitivity analysis was formulated as a systematical way to guide the optimization process. Sensitivity numbers were obtained for maximizing two different objective functions: output work and transmittance ratio. The results were satisfactory when compared with the sensitivity values obtained from an exhaustive numerical analysis.

Keywords: Fluid Actuator, Nonlinear, Topology Optimization, Sensitivity Analysis

1. INTRODUCTION

Morphing structures have been studied for developing reliable energy-efficient systems. Intending to achieve desirable features as high strength to self-weight ratio, simple controls, large and reversible shape changes and a wide range of service conditions, nastic plants have been taken as a major inspiration in this field [1-5]. Such plants are natural fluid actuators since they can actively reshape themselves by altering the pressure in their cells. In this context, the design of adaptive materials and mechanisms as bio-inspired cellular systems has been proposed.

Some authors work with biologically accurate models, *e.g.*, in the nastic material studied by Freeman & Weiland [1], the system's movement is provoked by a controlled transport of charge and fluid across cellular membranes. Others, like Pagitz et al. [2], work with more mechanical systems, in which the structures are deformed by directly controlling the pressure in the cells. In a more general

regard, some pneumatic actuators also fit in this second type of systems [6]. Those fluid-mechanical mechanisms have a fairly broad range of applications: propulsion devices, morphing aircraft wings, assistive wearable technologies.

This work aims for the design of pressure-actuated structures through topology optimization techniques. In the following sections, the class of problems to be considered and its finite element modeling are described. Afterward, a sensitivity analysis is explicitly developed, which allows a better understanding of the problem as a whole and serves to base future implementations of topology optimization methods, such as the Solid Isotropic Material with Penalization (SIMP) [7] and the Bidirectional Evolutionary Structural Optimization (BESO) [8].

Topology optimization methods are powerful tools for designing mechanisms [5, 9]. By simply defining the working domain, the objective function and some constraints, a broad range of possible solutions can be obtained. Considering structural problems under dependent loads, the BESO method has been successfully implemented on similar approaches for compliance minimization and optimization of frequency responses [10, 11].

Linear and nonlinear analysis may lead to dramatically different solutions when linear hypotheses are not attained [12]. Regarding the proposed fluid-actuators, nonlinear effects can be taken into account for improving the model's accuracy. There are geometrically nonlinear effects, since compliant mechanisms work under finite displacements [13]. Moreover, load nonlinearity is intrinsically present, since the loads depend on the deformed structure configuration. Apart from the more complex formulation for the finite element and optimization methods, those nonlinear effects act as hindering factors in terms of computational costs and convergence of the analysis. Provided that, besides the possible presence of critical points, multiple solutions and path-dependency, nonlinear systems have to be solved iteratively, by methods as Newton-Raphson and Arc Length [14].

Briefly, the objective of this work is to formulate the sensitivity analysis of the considered system and to validate this analytical formulation by comparing its results with the ones obtained from an exhaustive numerical analysis.

2. GENERAL DESCRIPTION

The schema on Figure 1 presents the main features of the proposed modeling for the fluid-actuator. The mechanism is defined by a domain Ω, by the areas $\Phi = \{\Phi_1, \Phi_2, ..., \Phi_n\} \subset \Omega$, by the imposed restrictions and by a set of springs $K = \{k_1, k_2, ..., k_m\}$.

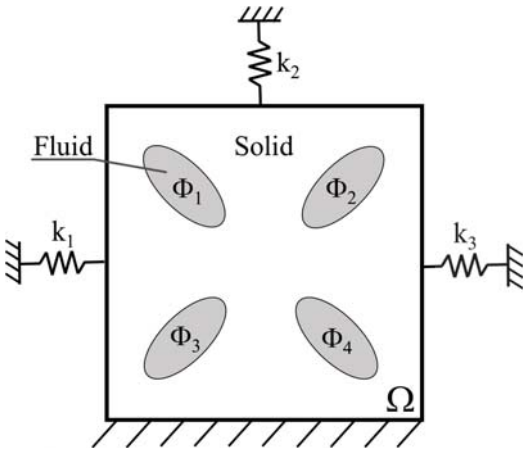

Figure 1. Proposed Fluid-Actuator

The areas Φ represent pressured fluid cavities, while the complementary domain, $\bar{\Omega} = \Omega - \Phi$, represents the solid structure. The imposed restrictions define which degrees of freedom should be fixed. In this illustration's example, the displacement field through the lower edge is set to zero.

The objective of the mechanism is defined by the springs K. Their positions, orientations and elastic constants are set so their total strain energy represents the output work of the actuator. In short, the mechanism's purpose is to transform, through a transmittance ratio, the available pressure energy into work.

The design of the actuator through topology optimization would be the determination of Φ that maximizes a chosen objective function. For this mechanism, it may be either the transmittance ratio or the output work.

3. STRUCTURAL MODEL

The proposed mechanism moves as the internal loads deform its structural part, which transmits the input energy to the springs. In order to accurately predict how the structure will deform for a given load, a geometrically nonlinear model was adopted.

3.1 Model Assumptions

A quasi-static loading, in which the process is reversible and isothermal, is considered. The system is assumed hyperelastic, *i.e.*, it exists an unique strain-energy density function ψ dependent only of the strain tensor E so that

$$\frac{\partial \psi}{\partial E} = S \tag{1}$$

where the conjugate stress tensor S also depends only on E. Which implies

$$\delta \psi = \langle S, \delta E \rangle \tag{2}$$

where $\langle \cdot, \cdot \rangle$ is the standard tensorial inner product and δ represents the virtual variation operator.

The solid material is considered continuum, homogeneous and isotropic. The constitutive law is assumed linear and elastic, defined by the Lamé parameters, λ and μ, as shown in Equation 3 (in indicial notation).

$$S_{ij} = \lambda E_{kk} \delta_{ij} + 2\mu E_{ij} \tag{3}$$

Lastly, the structure is considered bi-dimensional, in plane stress state.

3.2 Geometric Nonlinearity

The usual Hookean strain tensor $\bar{E}$ is not compatible for a structure under great displacements, because it neglects higher order terms that are not negligible when displacements are finite. This causes, *e.g.*, the incoherent result of having a body solely under rigid rotation and with a non-null strain tensor. $\bar{E}$ is given in Equation 4, where ∇u denotes the gradient matrix of the field of displacements within the domain.

$$\bar{E} = \frac{1}{2}\left(\nabla u + \nabla u^T\right) \tag{4}$$

For more appropriate tensors, the Seth class of Lagrangian strain tensors are considered [15]. Its general form is

$$\hat{E}^{(m)} = \begin{cases} \frac{1}{m}\left(U^m - I\right), & \forall m \in \mathbb{R}^* \\ \lim\limits_{m \to 0} \frac{1}{m}\left(U^m - I\right) = ln\left(U\right), & m = 0 \end{cases} \tag{5}$$

where U is the well known stretch tensor given by the polar decomposition of the deformation gradient. For this class of tensors, the desired behavior can be noted: the strain is not affected by rigid motions and it turns into the null tensor when there is no relative displacement between points of the body.

By using any of those strain tensors, the system acquires a nonlinear behavior, called geometrical in opposition to material nonlinearity, where the nonlinear aspect comes from the constitutive law.

Although the presented tensors are all suitable *a priori*, when considering a linear relation between the chosen strain and its conjugate stress, each choice of m will lead to a different model, that may correspond more or less with the real behavior of the physical structure.

The St. Venant-Kirchhoff ($m = 2$) and Hencky ($m = 0$) models have been commonly used to describe systems under finite displacements. However, the St. Venant-Kirchhoff model, which uses the Lagrangian Green strain $E_G = \hat{E}^{(2)}$, have unrealistic responses for large compressions. The preferable choice was the Hencky model, with the logarithmic strain $E_L = \hat{E}^{(0)}$, which can reasonably represent the behavior of realistic materials under great deformations [16, 17]. For a more compact notation, the logarithmic strain tensor will be noted simply as E in the subsequent sections.

4. LOADING CONSIDERATIONS

The proposed system works with a single pressure input for all cavities, the loading is quasi-static and there is no thermal effects. Those assumptions are enough to define how the fluid will behave in the mechanism.

Since dynamic effects are absent, the cavities' inner points are always at static equilibrium and do not weight in the analysis. The expansions and retractions of the cavities depend only on the solid-fluid interaction on the interfaces, which is a uniform hydrostatic loading. This means that the fluid does not need to be modeled, only the input pressure and the cavities geometry will act on the structure.

The loads' dependency on the shape of the deformed cavities configures a load nonlinearity, since the loading will be a function of the displacements field.

5. FINITE ELEMENT ANALYSIS

In this analysis, the chosen finite element was the four-node iso-parametric element. In order to represent the fluid interactions, dependent loads were included in the geometrically nonlinear structural model.

Regarding the considered optimization methods, a uniformly meshed domain is very desirable, so the possible topologies are not limited or somehow biased by the mesh. However, for square elements, the presence of multiple cutting edges and the amplification of cavities' perimeters may lead to unrealistic results for the uniformly meshed structure. To obtain more coherent results, a smoothing process is performed. After defining the fluid areas Φ on the meshed domain, each interface node pass through a filter, averaging its position with the ones of the nearby neighbors.

The equilibrium is given by the principle of virtual work [14], shown in Equation 6. It states that the energy variation provoked by a small virtual displacement variation δu is zero on static equilibrium.

$$\delta W = \delta W_{int} - \delta W_{ext} = 0 \tag{6}$$

The internal virtual work δW_{int} corresponds to the system's strain energy variation, relative to the deformation of both structure and set of springs. The external virtual work δW_{ext} corresponds to the work employed by the pressure loads on the cavities' interfaces.

The structural deformation term of the internal virtual work $\delta W_{int}^{(1)}$, shown in Equation 7, is given by the volumetric integration of $\delta\psi$ from Equation 2.

$$\delta W_{int}^{(1)} = \int_V \delta\psi \, dV = \int_V \langle S, \delta E \rangle \, dV \tag{7}$$

Considering that the spring forces in an element are given by the product of a diagonal matrix K by the nodal displacements vector u, the spring deformation term of the internal virtual work $\delta W_{int}^{(2)}$ is given by

$$\delta W_{int}^{(2)} = \langle Ku, \delta u \rangle \tag{8}$$

For a unitary width, the work employed on the perimeter of a fluid element due a virtual displacement is given by

$$\delta W_{ext} = p_o \, \delta A \tag{9}$$

where p_o is the input manometric pressure and δA is the virtual surface variation of the element. For the considered quadrilateral element, Equation 9 can be rewritten in function of u and of the nodal positions vector x, as presented on Equation 10.

$$\delta W_{ext} = \langle p_o F \left(x + u\right), \delta u \rangle \tag{10}$$

where F is the constant symmetric matrix presented below.

$$F = \frac{1}{2} \begin{bmatrix} 0 & 0 & 0 & 1 & 0 & 0 & 0 & -1 \\ 0 & 0 & -1 & 0 & 0 & 0 & 1 & 0 \\ 0 & -1 & 0 & 0 & 0 & 1 & 0 & 0 \\ 1 & 0 & 0 & 0 & -1 & 0 & 0 & 0 \\ 0 & 0 & 0 & -1 & 0 & 0 & 0 & 1 \\ 0 & 0 & 1 & 0 & 0 & 0 & -1 & 0 \\ 0 & 1 & 0 & 0 & 0 & -1 & 0 & 0 \\ -1 & 0 & 0 & 0 & 1 & 0 & 0 & 0 \end{bmatrix}$$

Combining the Equations 6, 7, 8 and 10, the equilibrium equation, in indicial notation, can be written as

$$\begin{aligned} \delta W = & \int_V S_{jk} \delta E_{jk} \, dV + K_{ij} u_j \delta u_i - p_o F_{ij} (x_j + u_j) \delta u_i = \\ & \left(\int_V S_{jk} \frac{\partial E_{jk}}{\partial u_i} \, dV + K_{ij} u_j - p_o F_{ij} (x_j + u_j) \right) \delta u_i = 0 \end{aligned} \tag{11}$$

Equation 11 must be satisfied for any small virtual displacement δu. Therefore, the left term, denoted as the residue Ψ, must be zero when the system is at static equilibrium. The considered unitary width reduces the volumetric integral to a surface integral. In indicial notation, the final equilibrium equation is

$$\Psi_i = \int_A S_{jk} \frac{\partial E_{jk}}{\partial u_i} \, dA + K_{ij} u_j - p_o F_{ij} (x_j + u_j) = 0_i \tag{12}$$

Since Ψ is a known function of u, the numerical problem is now fully described and the system behavior can be predicted by Equation 12. For the sequence, it will be useful to consider the residue terms separately as $\Psi_{int}^{(1)}$, $\Psi_{int}^{(2)}$ and Ψ_{ext} respectively.

The tangent stiffness matrix K_T is defined as

$$K_T = \frac{\partial \Psi}{\partial u} = \frac{\partial \Psi_{int}^{(1)}}{\partial u} + \frac{\partial \Psi_{int}^{(2)}}{\partial u} - \frac{\partial \Psi_{ext}}{\partial u} = K_{int}^{(1)} + K_{int}^{(2)} - K_{ext} \tag{13}$$

It can be seen that $K_{ext} = p_o F$ and $K_{int}^{(2)} = K$. As for $K_{int}^{(1)}$, it assumes a more complex form that will not be explicitly shown for conciseness.

To solve the system for multiple elements, an assembly operation is necessary. In next sections, the assembly of a given an elemental vector or matrix M will be noted $\lfloor M \rceil$, this operation also disregards restricted degrees of freedom.

6. SENSITIVITY ANALYSIS

Considering the meshed working domain, the mechanism's topology can be fully described by a vector X of elemental booleans x_e. For a each element e, $x_e = 0$ when it is fluid and $x_e = 1$ when it is solid. The topology optimization problem may then be written as

$$\begin{aligned} &\underset{X}{Maximize}\,(h(X)) \\ &Subject\ to: \sum_e x_e = N \\ &\forall e,\ x_e \in \{0,\ 1\} \end{aligned} \tag{14}$$

where h is the chosen objective function and N is the desired number of solid elements in the final topology. The Equations 15, 16 and 17 present the energy terms from which the objective functions can be defined.

$$W_{int}^{(1)} = \frac{1}{2} \sum_e \left[\int_A \langle S, E \rangle \, dA \right]_e \tag{15}$$

$$W_{int}^{(2)} = \frac{1}{2} \langle \lfloor Ku \rceil, \lfloor u \rceil \rangle \tag{16}$$

$$W_{ext} = W_{int}^{(1)} + W_{int}^{(2)} \tag{17}$$

Two objective functions were evaluated, the output work, given in Equation 18, and the transmittance ratio, given in Equation 19.

$$h_1 = W_{int}^{(2)} \tag{18}$$

$$h_2 = \frac{W_{int}^{(2)}}{W_{ext}} = \frac{W_{int}^{(2)}}{W_{int}^{(1)} + W_{int}^{(2)}} \tag{19}$$

A material penalization scheme is used so that the objective functions vary continuously with X [7]. By doing so, a sensitivity value can be assigned to each element e by differentiating the chosen objective function with respect to x_e, which now may assume any value between zero and one, including endpoints. Given a positive penalization exponent p, the following changes are proposed for turning the discrete model into a continuous one.

The Lamé parameters of each element are penalized so that the elemental stiffness decreases as x_e goes toward zero.

$$\begin{aligned} \lambda_e &= x_e^p \, \lambda \\ \mu_e &= x_e^p \, \mu \end{aligned} \tag{20}$$

And the matrix F of each element is penalized so that the pressure forces employed decreases as x_e goes toward one.

$$F_e = (1 - x_e^p) F \tag{21}$$

By using very high values for p, elements with intermediate values of x_e behave as fluid; while for p values near zero, elements with intermediate values of x_e behave as solid. For the present work, the chosen value was $p = 3$.

Thus, in indicial notation, the elemental sensitivity number α_e for the first objective function is given by

$$\alpha_e = \frac{\partial h_1}{\partial x_e} = \frac{1}{2} \frac{\partial \left(\lfloor K \rceil_{ij} \lfloor u \rceil_j \lfloor u \rceil_i \right)}{\partial x_e} = \lfloor K \rceil_{ij} \lfloor u \rceil_j \frac{\partial \lfloor u \rceil_i}{\partial x_e} \tag{22}$$

In order to remove the unknown term $\frac{\partial \lfloor u \rceil_i}{\partial x_e}$ from Equation 22, the objective function is substituted by the equivalent expression

$$\hat{h_1} = h_1 + \langle \Lambda, \lfloor \Psi \rceil \rangle \tag{23}$$

where Λ is an arbitrary vector, since Ψ is zero when the system is at static equilibrium. Therefore

$$\hat{\alpha_e} = \alpha_e + \frac{\partial \left(\Lambda_j \lfloor \Psi \rceil_j \right)}{\partial x_e} = \lfloor K \rceil_{ij} \lfloor u \rceil_j \frac{\partial \lfloor u \rceil_i}{\partial x_e} + \Lambda_j \frac{\partial \lfloor \Psi \rceil_j}{\partial x_e} \tag{24}$$

Using previous definitions, Equation 24 can be rewritten as

$$\begin{aligned} \hat{\alpha_e} = \lfloor \Psi_{int}^{(2)} \rceil_i \frac{\partial \lfloor u \rceil_i}{\partial x_e} + \Lambda_j \left(\frac{\partial x_e^p}{\partial x_e} \lfloor \Psi_{int}^{(1)} \rceil_j^e - \frac{\partial \left(1 - x_e^p \right)}{\partial x_e} \lfloor \Psi_{ext} \rceil_j^e + \lfloor K_T \rceil_{ji} \frac{\partial \lfloor u \rceil_i}{\partial x_e} \right) = \\ \left(\lfloor \Psi_{int}^{(2)} \rceil_i + \Lambda_j \lfloor K_T \rceil_{ji} \right) \frac{\partial \lfloor u \rceil_i}{\partial x_e} + p \, x_e^{p-1} \Lambda_j \left(\lfloor \Psi_{int}^{(1)} \rceil_j^e + \lfloor \Psi_{ext} \rceil_j^e \right) \end{aligned} \tag{25}$$

Here, the terms under the notation $\lfloor \cdot \rceil^e$ represent the elemental vectors in the global coordinate system.

By defining Λ as

$$\boxed{\Lambda = - \lfloor K_T \rceil^{-1} \lfloor \Psi_{int}^{(2)} \rceil} \tag{26}$$

the left term vanishes and Equation 25 becomes

$$\hat{\alpha_e} = p \, x_e^{p-1} \Lambda_j \left(\lfloor \Psi_{int}^{(1)} \rceil_j^e + \lfloor \Psi_{ext} \rceil_j^e \right) \tag{27}$$

Specially on discrete methods as BESO [8], sensitivity numbers have little quantitative meaning. Since it is used only comparatively, the obtained expression can be divided by a constant without any practical loss. Therefore, a normalized sensitivity number $\tilde{\alpha_e}$ may be defined as

$$\boxed{\tilde{\alpha}_e = \frac{1}{p}\hat{\alpha}_e = x_e^{p-1}\Lambda_j\left(\lfloor\Psi_{int}^{(1)}\rceil_j^e + \lfloor\Psi_{ext}\rceil_j^e\right) = x_e^{p-1}\langle\Lambda, \lfloor\Psi_{int}^{(1)}\rceil^e + \lfloor\Psi_{ext}\rceil^e\rangle} \tag{28}$$

Analogously, for maximizing the transmittance ratio, the new objective function $\hat{h_2}$ and the elemental sensitivity number $\hat{\beta}_e$ are given by

$$\hat{h_2} = h_2 + \langle\Upsilon, \lfloor\Psi\rceil\rangle \tag{29}$$

$$\hat{\beta}_e = \frac{\partial\hat{h_2}}{\partial x_e} \tag{30}$$

Following the same steps, the final expressions for the vector Υ and for the normalized elemental sensitivity number $\tilde{\beta}_e$ are

$$\boxed{\Upsilon = \lfloor K_T\rceil^{-1}\left(W_{int}^{(2)}\lfloor\Psi_{int}^{(1)}\rceil - W_{int}^{(1)}\lfloor\Psi_{int}^{(2)}\rceil\right)} \tag{31}$$

$$\boxed{\tilde{\beta}_e = \frac{(W_{ext})^2}{p}\hat{\beta}_e = x_e^{p-1}\Upsilon_j\left(\lfloor\Psi_{int}^{(1)}\rceil_j^e + \lfloor\Psi_{ext}\rceil_j^e\right) = x_e^{p-1}\langle\Upsilon, \lfloor\Psi_{int}^{(1)}\rceil^e + \lfloor\Psi_{ext}\rceil^e\rangle} \tag{32}$$

Having in mind a soft-kill BESO implementation [8], it was considered that $x_e = 0.01$ for fluid elements and $x_e = 1.00$ for solid elements. The results obtained from Equations 28 and 32 were validated with the ones obtained by exhaustively varying x_e for each element of the mesh and evaluating the objective functions variations. For this reason, to avoid massive processing times, a relatively coarse mesh was used.

The reference sensitivity numbers for the exhaustive analysis are given by Equations 33 and 34, in which the derivatives $\hat{\alpha}$ and $\hat{\beta}$ are numerically estimated.

$$\tilde{\alpha}_e^n = \frac{1}{p}\left(\frac{h_1(x_e) - h_1(x_{\bar{e}})}{x_e - x_{\bar{e}}}\right) \tag{33}$$

$$\tilde{\beta}_e^n = \frac{(W_{ext})^2}{p}\left(\frac{h_2(x_e) - h_2(x_{\bar{e}})}{x_e - x_{\bar{e}}}\right) \tag{34}$$

In the expressions above, $x_{\bar{e}}$ represents a value slightly inferior to x_e. The results presented in next section were obtained for $x_{\bar{e}} = x_e - 0.0001$.

7. RESULTS AND DISCUSSION

The Finite Element Method (FEM) implementation was validated by comparing results with the commercial software *ANSYS*. It is considered a cantilever beam of dimensions $1.00x0.02\,m$, discretized in a mesh of $400x8$ identical square elements. A vertical load of $250\,kN$ is applied at the center of the free extremity. The Young's modulus and Poisson's ratio of the material are, respectively, $E_y = 200\,GPa$ and $\nu = 0.3$. The width is unitary and the beam is on plane stress state.

The deformed structures obtained from linear and nonlinear analysis are presented on Figure 2. The linear structure behavior is an amplification of how the structure behaves under small displacements, therefore, it moves mostly vertically. On the other hand, the nonlinear structure has a much more realistic behavior, its displacement field is more complex and the volume distortions observed on the simpler case are reduced.

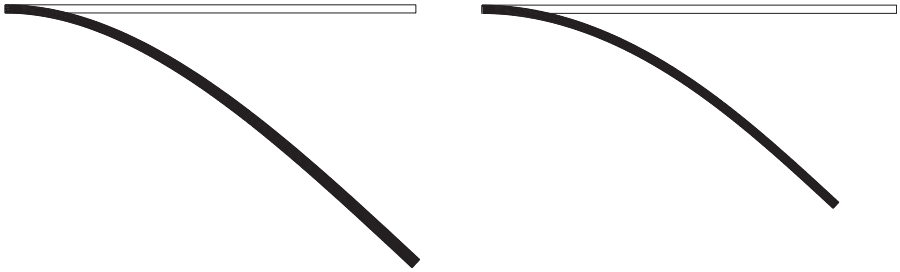

(a) (b)

Figure 2. FEM Solution: linear analysis (a); nonlinear analysis (b)

For both types of analysis, the maximal displacements obtained for the central node of the free extremity are presented on Table 1, as well as the reference values, from *ANSYS* simulation, and the percentage difference between them. On *ANSYS*, the geometrically nonlinear analysis is activated by the boolean "*NLGEOM*".

Table 1. FEM Validation – Comparison Between Maximal Displacements

Analysis Type	**Obtained**	**ANSYS**	**Difference**
Linear	0.6203 m	0.6203 m	0.00 %
Nonlinear	0.4956 m	0.4942 m	0.28 %

Although the mesh, the element type and the properties were the same, there was still a small difference for the nonlinear analysis. This probably comes from extra procedures performed by *ANSYS*, inaccessible to users. Anyway, such minor difference indicates that the method was well implemented and that the obtained results are reliable.

The following example was used for evaluating the sensitivity expressions presented. The mechanism is a vertical beam that actuates horizontally, pressing the spring placed on the upper extremity. The domain, the boundary conditions and the physical properties are shown on Figure 3.

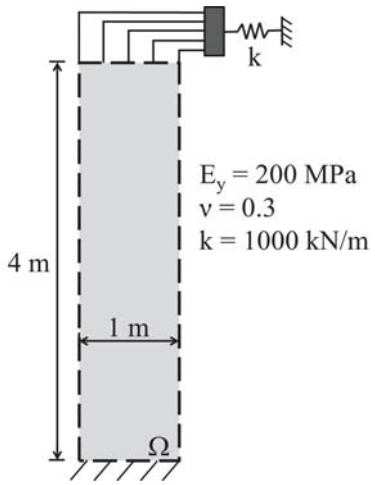

Figure 3. Mechanism Outline

A possible functional topology was proposed for the mechanism. Eight circular cavities, of radius $0.10\,m$, were distributed vertically on the left size of the structure. The domain was discretized in a mesh of $20x80$ square elements and the cavities were smoothed. The considered input was a positive manometric pressure of $25\,MPa$. The regular mesh, the smoothed one and the deformed structure under the given loading are presented on Figure 4.

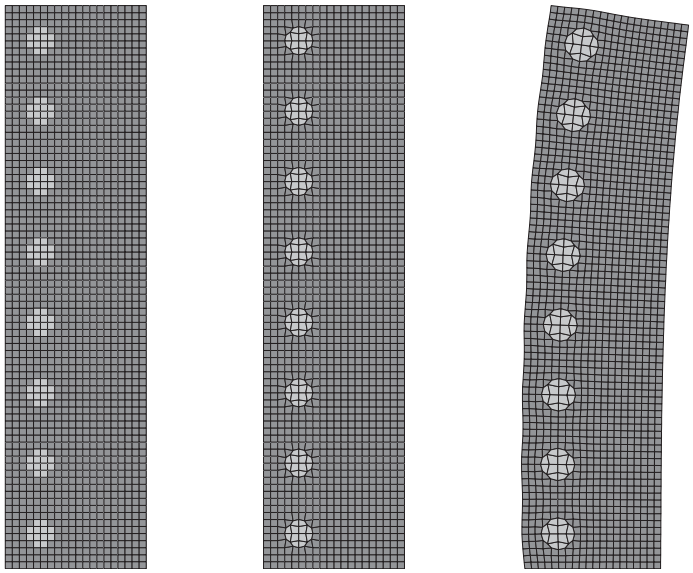

(a) (b) (c)

Figure 4. Considered Mesh with Solid (darker) and Fluid (lighter) Elements: regular and static (a); smoothed and static (b); smoothed and loaded (c)

The analytical sensitivity numbers obtained from Equations 28 and 32, as well as the numerical reference values estimated from Equations 33 and 34, are shown on Figure 5.

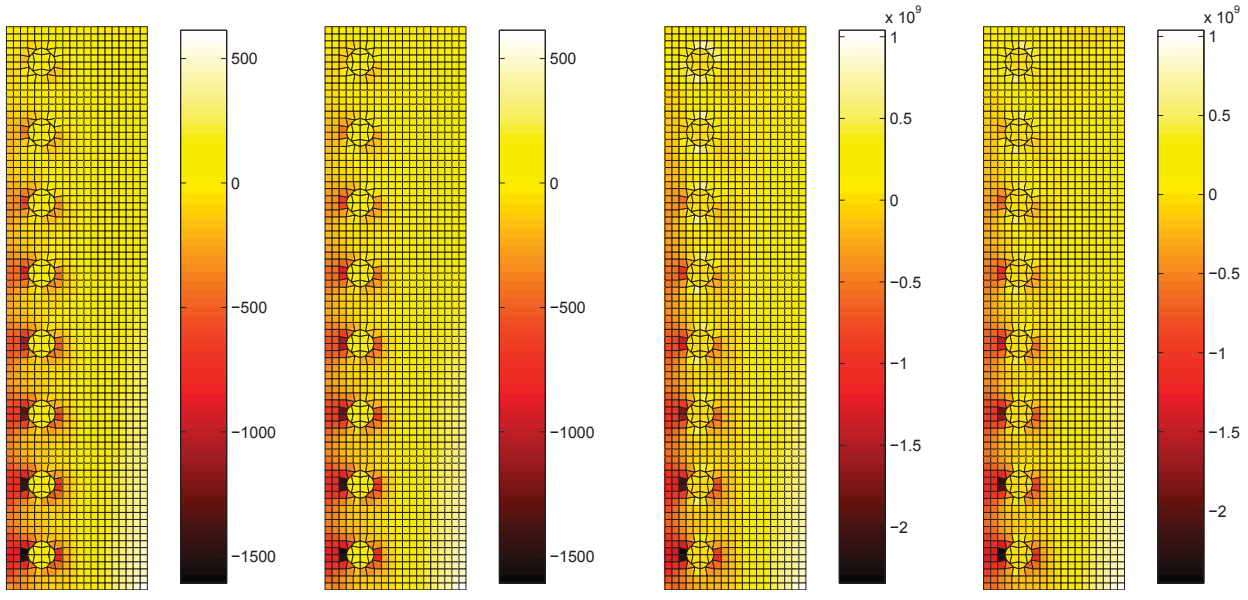

(a) (b) (c) (d)

Figure 5. Sensitivity Numbers for Output Work [analytical (a); numerical (b)] and for Transmittance Ratio [analytical (c); numerical (d)]

Although the quantitative values on the sensitivity maps have little relevance in the context of this work, the numerical scales were presented in order to show how similar the analytical and numerical results were. Regarding the results, the deducted formulation has been shown accurate.

Considering the optimization process, solid elements with negative sensitivity numbers are likely to be turned into fluid and fluid elements in high sensitivity areas are likely to be turned into solid. It can be seen that when the objective is the transmittance ratio, *i.e.*, the energy efficiency of the system, the sensitivity above and below each cavity is higher, as well as the sensitivity around the upper cavities. This indicates that optimal structures for maximizing output work will be different from the ones that maximize the transmittance ratio.

Under small loadings, the nonlinear effects are diminished. For highlighting the effects of the system's nonlinearity, the analysis was remade for a pressure input of $2\,kPa$ and compared with the previous result. For both loadings, the sensitivity maps for transmittance maximization are shown on Figure 6.

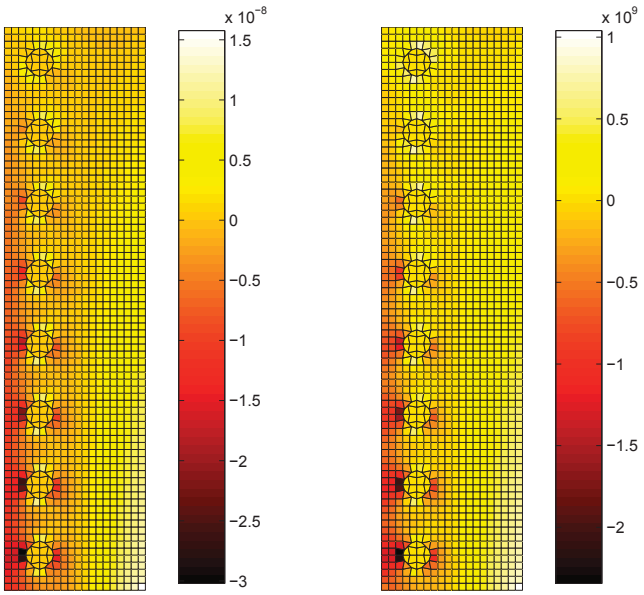

(a) (b)

Figure 6. Sensitivity Numbers for Transmittance Ratio under 2 kPa (a) and 25 MPa (b)

Apart from the different numerical values, the sensitivity distribution is affected by the loading variation. Specially around the upper cavities, the sensitivity values for the small loading are reduced when compared with the case under high pressure. It means that the nonlinear behavior will affect the elements' relevance on the objective function and should also lead to distinct optimal structures.

8. CONCLUSIONS

A scheme for a bio-inspired fluid actuator was proposed. Its finite element model was developed considering two nonlinear aspects: geometric nonlinearity and load nonlinearity. Regarding the design of such mechanisms through topology optimization techniques, a sensitivity analysis was formulated.

The finite element model was validated through comparison with a commercial software. And the sensitivity analysis was validated through comparison with an exhaustive numerical evaluation. The results were satisfactory for both procedures.

As following steps, optimized structures should be obtained by using the presented sensitivity analysis in topology optimization methods.

REFERENCES

[1] Freeman, E. and Weiland, L. M. (2009). "High energy density nastic materials: parameters for tailoring active response." Journal of Intelligent Material Systems and Structures, 20(2):233–243.

[2] Pagitz, M., Lamacchia, E., and Hol, J. (2012). "Pressure-actuated cellular structures." Bioinspiration & biomimetics, 7(1):016007.

[3] Lv, J., Liu, H., and Zhang, H. (2014). "A multiscale co-rotational method for geometrically nonlinear shape morphing of 2D fluid actuated cellular structures." Mechanics of Materials, 79:1–14.

[4] Lv, J., Zhang, H., and Chen, B. (2014). "Shape and topology optimization for closed liquid cell materials using extended multiscale finite element method." Structural and Multidisciplinary Optimization, 49(3):367–385.

[5] Lv, J., Tang, L., Li, W., Liu, L., and Zhang, H. (2016). "Topology optimization of adaptive fluid-actuated cellular structures with arbitrary polygonal motor cells." Smart Materials and Structures, 25(5):055021.

[6] Agarwal, G., Besuchet, N., Audergon, B., and Paik, J. (2016). "Stretchable Materials for Robust Soft Actuators towards Assistive Wearable Devices." Scientific reports, 6.

[7] Bendsøe, M. P. and Sigmund, O. (1999). "Material interpolation schemes in topology optimization." Archive of applied mechanics, 69(9):635–654.

[8] Huang, X. and Xie, M. (2010). Evolutionary topology optimization of continuum structures: methods and applications. John Wiley & Sons.

[9] Maute, K. and Frangopol, D. M. (2003). "Reliability-based design of MEMS mechanisms by topology optimization." Computers & Structures, 81(8):813–824.

[10] Vicente, W., Picelli, R., Pavanello, R., and Xie, Y. (2015). "Topology optimization of frequency responses of fluid–structure interaction systems." Finite Elements in Analysis and Design, 98:1–13.

[11] Picelli, R., Vicente, W., and Pavanello, R. (2015). "Bi-directional evolutionary structural optimization for design-dependent fluid pressure loading problems." Engineering Optimization, 47(10):1324–1342.

[12] Bruns, T. E. and Tortorelli, D. A. (2001). "Topology optimization of non-linear elastic structures and compliant mechanisms." Computer Methods in Applied Mechanics and Engineering, 190(26):3443–3459.

[13] Cunha, D. C. and Pavanello, R. (2016). "Evolutionary Topology Optimization of Geometrically Nonlinear Continuum Structures." In XXIV Congresso de Iniciação Científica da Unicamp.

[14] De Borst, R., Crisfield, M. A., Remmers, J. J., and Verhoosel, C. V. (2012). Nonlinear finite element analysis of solids and structures. John Wiley & Sons.

[15] Seth, B. (1961). "Generalized strain measure with applications to physical problems." Technical report, DTIC Document.

[16] Plešek, J. and Kruisová, A. (2006). "Formulation, validation and numerical procedures for Hencky's elasticity model." Computers & structures, 84(17):1141–1150.

[17] Xiao, H. (2005). "Hencky strain and Hencky model: extending history and ongoing tradition." Multidiscipline Modeling in Materials and Structures, 1(1):1–52.

RESPONSIBILITY NOTICE

The authors are the only responsible for the printed material included in this paper.